

# Ultraviolet avalanche in anisotropic non-Abelian plasmas

Adrian Dumitru<sup>a</sup>, Yasushi Nara<sup>a</sup> and Michael Strickland<sup>b</sup>

<sup>a</sup> *Institut für Theoretische Physik, Johann Wolfgang Goethe Universität,  
Max von Laue Str. 1, D-60438 Frankfurt am Main, Germany*

<sup>b</sup> *Frankfurt Institute for Advanced Study,  
Johann Wolfgang Goethe Universität, Max von Laue Str. 1,  
D-60438 Frankfurt am Main, Germany*

(Dated: May 25, 2019)

## Abstract

We present solutions of coupled particle-field evolution in classical  $U(1)$  and  $SU(2)$  gauge theories in real time on three-dimensional lattices. For strongly anisotropic particle momentum distributions, we find qualitatively different behavior for the two theories when the field strength is high enough that non-Abelian self-interactions matter for  $SU(2)$ . It appears that the energy drained by a Weibel-like plasma instability from the particles does not build up exponentially in transverse magnetic fields but instead returns, isotropically, to the hard scale via a rapid avalanche into the ultraviolet.

## I. INTRODUCTION

One of the most important open questions emerging from the Relativistic Heavy-Ion Collider (RHIC) program is how quickly, and by what process, the stress-energy tensor of the high-density QCD matter produced in the central rapidity region becomes isotropic. This is important, for example, to determine the maximal temperature achieved in such collisions, which will also be pursued in the near future at even higher energies at the CERN Large Hadron Collider (LHC).

One of the chief obstacles to thermalization in ultrarelativistic heavy-ion collisions is the rapid longitudinal expansion of the central rapidity region. If the matter expands too quickly then there will not be sufficient time for its constituents to interact and thermalize. In the absence of interactions, the longitudinal expansion causes the system to become much colder in the longitudinal direction than in the transverse directions, corresponding to  $\langle p_L^2 \rangle \ll \langle p_T^2 \rangle$  in the local rest frame. One can then ask how long it would take for interactions to restore isotropy in momentum space.

High-energy heavy-ion collisions release a large amount of partons from the wavefunctions of the colliding nuclei. Partons with very large transverse momenta originate from high- $Q^2$  hard interactions, while partons with transverse momenta below the so-called saturation momentum  $Q_s$  (given by the square root of the color charge density per unit area in the incoming nuclei) are much more abundant and are better viewed as a classical non-Abelian field [1, 2, 3]. At high energies,  $Q_s \gg \Lambda_{\text{QCD}}$  sets a semi-hard scale which allows for a weak-coupling treatment of the early-stage dynamics. However, due to the large occupation number of the soft modes below  $Q_s$  (the classical color field has strength  $F_{\mu\nu} \sim 1/g$ ), the problem is nevertheless non-perturbative.

The evolution following the initial impact was among the questions which the so-called “bottom-up scenario” [4] attempted to answer. For the first time, it addressed the dynamics of soft modes (“fields”) with momenta much below  $Q_s$  coupled to the hard modes (“particles”) with momenta on the order of  $Q_s$  and above. However, it has emerged recently that one of the assumptions made in this model is not correct. The debate centers around the very first stage of the bottom-up scenario in which it was assumed that (a) collisions between the high-momentum (or hard) modes were the driving force behind isotropization and that (b) the low-momentum (or soft) fields were assumed to act only to screen the electric interaction. In doing so, the bottom-up scenario implicitly assumed that the underlying soft gauge modes behaved the same in an anisotropic plasma as in an isotropic one. However, it turns out that in anisotropic plasmas, within the so-called “hard loop approximation” (see below), the most important collective mode corresponds to an instability of transverse magnetic field fluctuations [5, 6, 7]. Recent works have shown that the presence of these instabilities is generic for distributions which possess a momentum-space anisotropy [8, 9, 10] and have obtained the full hard-loop (HL) action in the presence of an anisotropy [11].

In the last year there have been significant advances in the understanding of non-Abelian soft-field dynamics in anisotropic plasmas within the HL framework [12, 13]. The HL framework is equivalent to the collisionless Vlasov theory of eikonized hard particles, i.e. the particle trajectories are assumed to be unaffected by the induced background field. It is strictly applicable only when there is a large scale separation between the soft and hard momentum scales<sup>1</sup>. Even with these simplifying assumptions HL gauge dynamics is non-trivial

---

<sup>1</sup> Of course, in the hard-loop approach very small angle deflections,  $\theta \sim g$ , are included self-consistently.

due to the presence of non-linear interactions which can act to regulate unstable growth. These non-linear interactions become important when the vector potential amplitude is on the order of  $A_{\text{non-Abelian}} \sim p_{\text{soft}}/g \sim (gp_h)/g$ , where  $p_h$  is the characteristic momentum of the hard particles<sup>2</sup>. In QED there is no such complication and the fields grow exponentially until  $A_{\text{Abelian}} \sim p_h/g$  at which point the hard particles undergo large-angle deflections by the soft background field invalidating the assumptions underpinning the hard-loop effective action.

Recent numerical studies of HL gauge dynamics for SU(2) gauge theory indicate that the gauge field dynamics changes from exponential field growth indicative of a conventional Abelian plasma instability to linear growth when the vector potential amplitude reaches the non-Abelian scale,  $A_{\text{non-Abelian}} \sim p_{\text{hard}}$  [12, 13]. This linear growth regime is characterized by a cascade of the energy pumped into the soft modes by the instability to higher-momentum plasmon-like modes [23, 24]. These results indicate that there is a fundamental difference between Abelian and non-Abelian plasma instabilities. However, even with this new understanding the HL framework relies on the existence of a large separation between the hard and soft momentum scales by design. One would like to know what happens when the scale separation between hard and soft modes is not very large or when the initial fields have large (non-linear) amplitudes which is the situation faced in real experiments. In this case one is naturally led to consider instead the Wong-Yang-Mills (WYM) equations. These equations can be shown to reproduce the HL effective action in the linear weak-field approximation [25, 26, 27]; however, when solved fully they go beyond the HL approximation.

In this paper we present first real-time three-dimensional lattice results obtained by solution of the WYM equations for coupled U(1) and SU(2) particle-field systems. For SU(2) gauge group, the WYM equations describe the propagation of classical colored particles in a colored background field in a framework that self-consistently includes the deflection of the hard particles by the soft fields. In practice, the equations are solved using the test-particle method and we present an improved numerical algorithm which uses current smearing to enable us to obtain convergent results with much fewer test particles than the straightforward “nearest grid point” (point particle) method. We focus here on simulations with large anisotropies of the particles and, for SU(2), on initial field strengths beyond the non-Abelian scale.

Our numerical results agree in some qualitative aspects with the HL calculations in that we see a transfer of energy from particles to the soft fields which saturates at late times. However, for the simulations presented here, the saturation seems to stem from a rapid “avalanche” of energy which has been dumped in soft modes to higher momentum modes. Due to finite lattice spacing this avalanche stops at the highest momentum modes of our lattice at which time the rapid growth of the field energy density ends. As the lattice spacing in our simulations is decreased we find that the amplitude at which the field energy density saturates increases, indicating that the mechanism for saturation is the rapid population of hard lattice modes. This is the main difference to the cascade which occurs in hard-loop simulations with moderate anisotropies [24], where field modes near the hard particle scale do not get populated until parametrically large times. The behavior seen here might be related to the chaoticity of three-dimensional classical Yang-Mills fields [28, 29, 30]. Additional

---

<sup>2</sup> We will not attempt here to use the specific fields obtained from the Color Glass Condensate wave functions [14, 15, 16, 17, 18, 19, 20, 21, 22] as initial conditions. Hence, we label the hard particle momentum scale more generically as  $p_h$  rather than  $Q_s$ .

studies are necessary, however, before firm conclusions in that regard can be drawn.

In Sec. II we present the Wong-Yang-Mills equations and the basics of the test particle method. In Sec. III we discuss the numerical methods employed. In Sec. IV we present results for U(1) and SU(2) gauge theories. In Sec. V we discuss the implications of our results and list open questions which remain.

## II. WONG-YANG-MILLS EQUATIONS

In this paper we present solutions of the classical Vlasov transport equation for hard gluons with non-Abelian color charge  $q^a$  in the collisionless approximation [31, 32],

$$p^\mu [\partial_\mu - g q^a F_{\mu\nu}^a \partial_p^\nu - g f_{abc} A_\mu^b q^c \partial_{q^a}] f(x, p, q) = 0 . \quad (2.1)$$

Here,  $f(t, \mathbf{x}, \mathbf{p}, q^a)$  denotes the single-particle phase space distribution function and  $g$  is the gauge coupling, which can take arbitrary values at the classical level.

The Vlasov equation is coupled self-consistently to the Yang-Mills equation for the soft gluon fields,

$$D_\mu F^{\mu\nu} = J^\nu = g \int \frac{d^3 p}{(2\pi)^3} dq q v^\nu f(t, \mathbf{x}, \mathbf{p}, q) , \quad (2.2)$$

with  $v^\mu \equiv (1, \mathbf{p}/p)$  the four-velocity of a particle divided by the Lorentz  $\gamma$ -factor. These equations reproduce the ‘‘hard thermal loop’’ effective action near equilibrium [25, 26, 27]. However, the full classical transport theory (2.1,2.2) also reproduces some higher  $n$ -point vertices of the dimensionally reduced effective action for static gluons [33] beyond the hard-loop approximation. The back-reaction of the long-wavelength fields on the hard particles (‘‘bending’’ of their trajectories) is, of course, taken into account, which is important for understanding particle dynamics in strong fields.

Eq. (2.1) can be solved numerically by replacing the continuous single-particle distribution  $f(\mathbf{x}, \mathbf{p}, q)$  by a large number of test particles:

$$f(\mathbf{x}, \mathbf{p}, q) = \frac{1}{N_{\text{test}}} \sum_i \delta(\mathbf{x} - \mathbf{x}_i(t)) (2\pi)^3 \delta(\mathbf{p} - \mathbf{p}_i(t)) \delta(q^a - q_i^a(t)) , \quad (2.3)$$

where  $\mathbf{x}_i(t)$ ,  $\mathbf{p}_i(t)$  and  $q_i^a(t)$  are the coordinates of an individual test particle and  $N_{\text{test}}$  denotes the number of test-particles per physical particle. The *Ansatz* (2.3) leads to Wong’s equations [31, 32]

$$\frac{d\mathbf{x}_i}{dt} = \mathbf{v}_i, \quad (2.4)$$

$$\frac{d\mathbf{p}_i}{dt} = g q_i^a (\mathbf{E}^a + \mathbf{v}_i \times \mathbf{B}^a), \quad (2.5)$$

$$\frac{dq_i}{dt} = ig v_i^\mu [A_\mu, \mathbf{q}_i], \quad (2.6)$$

$$J^{a\nu} = \frac{g}{N_{\text{test}}} \sum_i q_i^a v^\nu \delta(\mathbf{x} - \mathbf{x}_i(t)). \quad (2.7)$$

for the  $i$ -th test particle. The time evolution of the Yang-Mills field can be followed by the standard Hamiltonian method [34] in  $A^0 = 0$  gauge. Specific numerical algorithms to solve the classical field equations coupled to particles shall be presented in the next section.

We use the following dimensionless lattice variables:

$$\mathbf{E}_L^a = \frac{ga^2}{2} \mathbf{E}^a, \quad \mathbf{p}_L = \frac{a}{4} \mathbf{p}, \quad Q_L^a = \frac{1}{2} q^a, \quad N_{\text{test},L} = \frac{N_{\text{test}}}{g^2}. \quad (2.8)$$

Our lattice Hamiltonian is then

$$H_L = \frac{1}{2} \sum_i \mathbf{E}_{i,L}^{a,2} + \frac{1}{2} \sum_{\square} (N_c - \text{Re Tr } U_{\square}) + \frac{1}{N_{\text{test},L}} \sum_j |\mathbf{p}_{j,L}|, \quad (2.9)$$

which is related to the physical Hamiltonian by  $H = (4/g^2 a) H_L$ . To convert lattice variables to physical units we fix the length of the lattice to  $L = 5$  fm which then determines the physical scale for the lattice spacing  $a$ . All other dimensionful quantities can then be converted to physical units using eqs. (2.8).

For most of the results presented here the initial phase-space distribution of hard gluons is taken to be a (parity-invariant) planar momentum distribution:

$$f(\mathbf{p}) = n_g \left( \frac{2\pi}{p_h} \right)^2 \delta(p_z) \exp(-p_T/p_h), \quad (2.10)$$

with  $p_T = \sqrt{p_x^2 + p_y^2}$  and  $n_g$  the number density of hard gluons (summed over two helicities and, for  $SU(N_c)$  gauge group, also over  $N_c^2 - 1$  color states). This represents a quasi-thermal distribution in two dimensions, with average momentum equal to  $p_h$ . At the initial time  $t = 0$  we randomly sample  $N_p = N_{\text{test}} n_g a^3$  particles from the distribution (2.10) at each cell of the lattice<sup>3</sup>.

We shall also present data for distributions with more moderate or vanishing anisotropy for numerical checks, where indicated. In lattice units,  $p_{h,L}$  should not be much smaller than 1; otherwise, the particle and field modes would overlap significantly. Instead of the number density  $n_g$  of hard gluons it is also customary to quote the assumed value for the mass scale

$$m_{\infty}^2 = g^2 N_c \int \frac{d^3 p}{(2\pi)^3} \frac{f(\mathbf{p})}{|\mathbf{p}|} \sim g^2 N_c \frac{n_g}{p_h}. \quad (2.11)$$

(For the particular distribution (2.10) the latter is actually an equality.) This quantity sets the scale for the growth rate of unstable field modes in the linear approximation.

The initial field amplitudes are sampled from a Gaussian distribution with a width tuned to a given initial energy density:

$$\langle A_i^a(\mathbf{x}) A_j^b(\mathbf{y}) \rangle = \frac{4\mu^2}{g^2} \delta_{ij} \delta^{ab} \delta(\mathbf{x} - \mathbf{y}), \quad (2.12)$$

and  $\mathbf{E} = -\dot{\mathbf{A}} = 0$ . Gauss's law then implies that the local charge density at time  $t = 0$  vanishes. We ensure that any particular initial condition satisfies *exact* local charge neutrality. In our  $U(1)$  simulations we monitor the time evolution of Gauss's law as a check of the numerical accuracy. Our charge smearing algorithm for  $SU(2)$ , on the other hand,

---

<sup>3</sup> When  $N_p$  is not very large it is useful to ensure explicitly that the sum of particle momenta in each cell vanishes, for example by adjusting the momentum of the last particle accordingly.

explicitly exploits (covariant) current conservation and hence Gauss’s law is satisfied exactly by construction.

Observables should finally be averaged over several initial field and particle configurations. Due to limited computational resources, we shall mostly stick to a single simulation run. However, we here consider only observables which are averages over the entire lattice and so do not fluctuate very much for runs with different initial seed.

### III. NUMERICAL METHODS

#### A. NGP method for non-Abelian gauge theories

We first summarize the method developed in Ref. [35, 36] where zero-order weighting is used (i.e., point particles). In that approach, one simply counts the number of particles within a cell to determine the charge density, which is why it is called the nearest-grid-point (NGP) method. A current is generated only when a particle crosses a cell boundary from  $i$  to  $i + 1$ . This induces a current on that link which is  $J(i) = Q\delta(t - t_{\text{cross}})/N_{\text{test}}$ . In order to satisfy the lattice covariant continuity equation,

$$\dot{\rho}_i = \sum_x U_x^\dagger(i-x)J_x(i-x)U_x(i-x) - J_x(i) , \quad (3.1)$$

the charge must be parallel transported:

$$Q(i+1) = U_x^\dagger(i)Q(i)U_x(i) . \quad (3.2)$$

The rotation of the particle’s momentum by the magnetic field can be updated continuously but its magnitude changes only when it crosses a link. The momentum “kick” can be determined by energy conservation:

$$|\mathbf{p}_{\text{ini}}| + \frac{N_{\text{test}}}{2} \mathbf{E}_{\text{ini}}^2 = |\mathbf{p}_{\text{fin}}| + \frac{N_{\text{test}}}{2} (\mathbf{E}_{\text{ini}} - J)^2 . \quad (3.3)$$

Substituting  $J = Q/N_{\text{test}}$  and assuming that the particle crosses the cell boundary in  $x$ -direction, one obtains

$$|\mathbf{p}_{\text{fin}}| = |\mathbf{p}_{\text{ini}}| - E_{x,\text{ini}}Q + Q^2/(2N_{\text{test}}) . \quad (3.4)$$

This way, the total energy

$$E_{\text{tot}} = \frac{1}{2} \sum_{\text{lattice}} (\mathbf{E}^2 + \mathbf{B}^2) + \frac{1}{N_{\text{test}}} \sum_i |\mathbf{p}_i| \quad (3.5)$$

is conserved.

In principle, time ordering of the link crossings by particles is required [35, 36] in every time step, which becomes very time consuming when the number of test-particles is large. However, we have found that at least for our present purposes time-ordering does not affect our results significantly and so will be ignored in what follows.

This method was applied in [37, 38, 39] to study a simplified situation with fields and particles living on a one-dimensional spatial lattice. Physically, this corresponds to a transversally homogeneous system (translational invariance in  $x$  and  $y$  directions). For such 1d-3v

simulations<sup>4</sup> the current can be made sufficiently smooth by employing enough test-particles. Ref. [37, 38, 39] found that the currents were sufficiently smooth when the number of particles per lattice site,  $N_p = N_{\text{test}} n_g a^3$ , was on the order of a few hundred to a thousand.

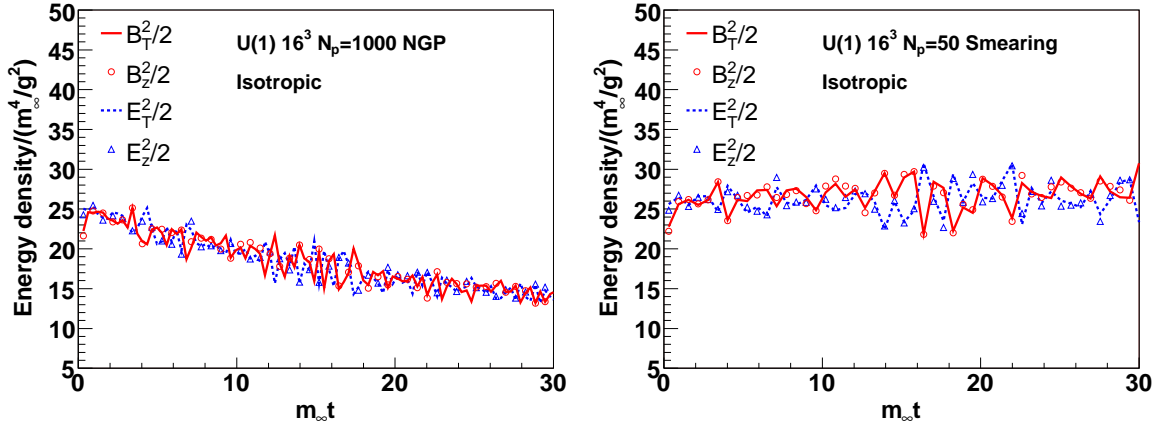


FIG. 1: Time evolution of the magnetic and electric energy densities for  $U(1)$  gauge group and isotropic particle momentum distribution using the nearest-grid-point method (left) and smeared-particles (right).

Full 3d-3v simulations, however, require improved algorithms since 3d lattices have many more sites and the NGP method becomes computationally too expensive. In Fig. 1 (left), the time evolution of the field energy densities on a  $16^3$  lattice with  $N_p = 1000$  test-particles per site are shown. Despite the large number of particles, there seems to be an anomalous damping of the fields with the NGP method. We naively expect that to achieve the same accuracy as for a one-dimensional lattice,  $N_p$  would have to increase exponentially with the number of spatial dimensions:  $N_p^{3d} \sim (N_p^{1d})^3$ . This makes multi-dimensional NGP simulations practically impossible and forces one to consider methods for smoothing particle densities and currents.

## B. Current smearing in electromagnetic PIC simulations

In Abelian plasmas it is common to employ smoothed currents for particle-in-cell (PIC) simulations [40, 41] in order to avoid numerical noise. The charge density at site  $(i, j, k)$  is obtained by smearing<sup>5</sup>

$$\rho(i, j, k) = e \sum_{n=1}^{N_p} S_i(x_n) S_j(y_n) S_k(z_n) . \quad (3.6)$$

Here,  $S$  is a form factor. For example, the first-order form factor (shape-factor) is

$$S_i(\xi) = \begin{cases} 1 - |\xi - i| & \text{for } |\xi - i| \leq 1, \\ 0 & \text{for } |\xi - i| > 1 \end{cases} \quad (3.7)$$

<sup>4</sup> Fields and charge densities fluctuate only in  $z$ -direction but particle velocities can point in any direction.

<sup>5</sup> We assume  $\Delta x = \Delta y = \Delta z = 1$ .

However, it is well known that if we naively define the current density at each grid point as

$$J_\alpha(i, j, k) = e \sum_{n=1}^{N_p} v_{\alpha,n} S_i(x_n) S_j(y_n) S_k(z_n), \quad \alpha = x, y, z, \quad (3.8)$$

then the continuity equation is not satisfied exactly [40, 41], requiring us to correct the electric field by solving the Poisson equation.

To avoid solving Poisson's equation in each time step, several numerical techniques for solving the continuity equation have been developed [42, 43, 44, 45, 46]. For simplicity, we consider the 2d problem to explain how to satisfy local charge conservation in electromagnetism. We consider a particle moving from  $(x_1, y_1)$  to  $(x_2, y_2)$  during a time step  $\Delta t$ , i.e.  $x_2 = x_1 + v_x \Delta t$ ,  $y_2 = y_1 + v_y \Delta t$ . We also restrict ourselves to the case in which  $(x_2, y_2)$  belongs to the same lattice site  $(i, j)$ . Charge conservation of the assigned current densities is realized with the procedure described by Eastwood [42],

$$\begin{aligned} J_x(i, j) &= F_x(1 - W_y), & J_x(i, j + 1) &= F_x W_y, \\ J_y(i, j) &= F_y(1 - W_x), & J_y(i + 1, j) &= F_y W_x, \end{aligned} \quad (3.9)$$

where  $(F_x, F_y) \equiv \mathbf{F}$  represents the charge flux

$$F_x = e \frac{x_2 - x_1}{\Delta t}, \quad F_y = e \frac{y_2 - y_1}{\Delta t}. \quad (3.10)$$

$W$  represents the first-order shape-factor corresponding to the linear weighting function defined at the midpoint between the starting point  $(x_1, y_1)$  and the end point  $(x_2, y_2)$

$$W_x = \frac{x_1 + x_2}{2} - i, \quad W_y = \frac{y_1 + y_2}{2} - j. \quad (3.11)$$

One can easily show that the lattice continuity equation

$$J_x(i, j) - J_x(i - 1, j) + J_y(i, j) - J_y(i, j - 1) = \frac{\rho^t(i, j) - \rho^{t+\Delta t}(i, j)}{\Delta t}. \quad (3.12)$$

is satisfied with the definition (3.9) of the current. When  $(x_2, y_2)$  is a different lattice site than the original  $(i, j)$  one, we use the 'Zigzag scheme' developed in Ref. [46].

Much of the numerical noise is already eliminated by such linear interpolation. As a further step to smoother currents, we also average over adjacent neighboring cells (in all three dimensions) [47]. Specifically, the flux arrays are shared with the weight  $(1/4, 1/2, 1/4)$ . This means that each flux is spread over  $3 \times 3 \times 3$  neighboring cells and each particle has to refer  $12 \times 27 = 324$  cells. Finally, we note that for consistency the electromagnetic forces should be smeared in a similar way as the currents when a particle momentum is updated. The momentum update itself is explained in appendix A.

In Fig. 1 (right) we show the  $U(1)$  energy densities resulting from an isotropic run using  $N_p = 50$  smeared test-particles per site. As can be seen from this figure the smeared-particle result does not suffer from the anomalous damping seen with the NGP method. More importantly, this result was obtained using many fewer particles than would be required to obtain a stable NGP result. Therefore the smeared-particle method makes three-dimensional colored-particle-cell (CPIC) simulations possible in practice.

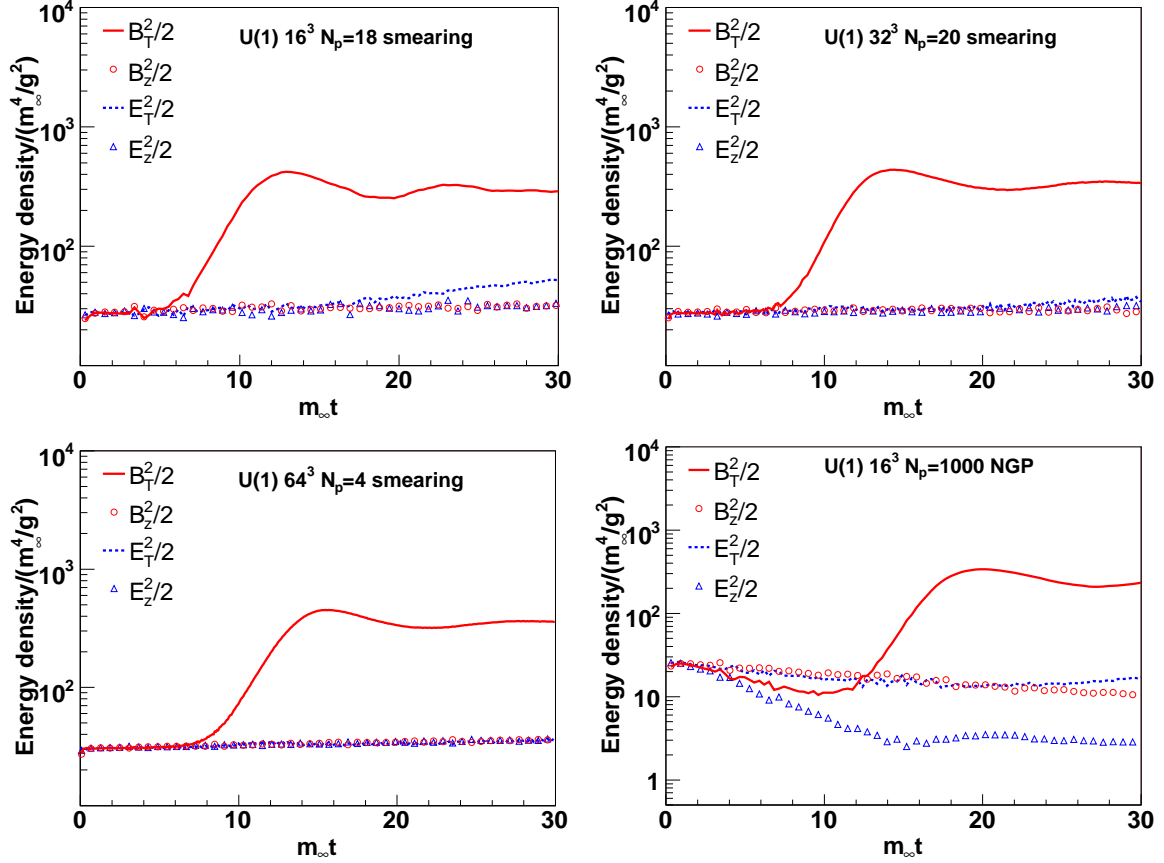


FIG. 2: Time evolution of the field energy densities for  $U(1)$  gauge group and anisotropic particle momentum distribution (2.10) on  $16^3$ ,  $32^3$  and  $64^3$  lattices. Simulation parameters are  $L = 5$  fm,  $p_h = 16$  GeV,  $g^2 n_g = 20$  fm $^{-3}$ ,  $m_\infty = 0.22$  GeV.

Fig. 2 shows the  $U(1)$  field energy densities as a function of time for the anisotropic initial particle momentum distribution using both smeared particles and the NGP method. These simulations illustrate the improved accuracy of the smearing method as compared to the NGP method. Moreover, thanks to the smaller number of test-particles required by the smearing method we are now able to also run simulations on larger lattices. For these initial conditions, we observe an instability for transverse magnetic fields while all other field amplitudes are essentially constant over the depicted time interval. We also note that the evolution of the fields is essentially independent of the lattice spacing, indicating that only soft field modes are important for the dynamics of the instability in the Abelian theory. Below, we shall find that the situation is different for non-Abelian fields.

The growing fields deflect the particles if their momenta are not asymptotically large so that they acquire non-vanishing longitudinal momenta  $p_z$  (c.f. section IV). We remark that PIC methods are not well suited for simulations of the extreme weak-field limit, where the particles propagate on nearly straight-line trajectories for a very long time.<sup>6</sup> This is not due to physical but technical limitations: the weaker the fields, the more accurate the particle current  $J^\nu$  needs to be (for example with respect to cancellations of positively and negatively

<sup>6</sup> This is better done within the hard-loop approximation.

charged particles etc.), as it represents a source-term in the field equations. High-precision currents, in turn, can only be achieved by employing a large number of test particles, driving up the computational time. In practice, the weakest fields for which simulations were feasible correspond to initial energy densities of about  $0.1 m_\infty^4/g^2$  for  $U(1)$  and  $\sim 10 m_\infty^4/g^2$  for  $SU(2)$  gauge group, respectively. The natural regime of applicability of PIC methods is when the separation between hard and soft degrees of freedom is not asymptotically large.

### C. PIC simulations in non-Abelian gauge theories

A straightforward extension of the above-mentioned smearing method to the non-Abelian case would be to define the current as

$$J_x(i, j) = Q \frac{x_2 - x_1}{\Delta t} (1 - W_y), \quad J_x(i, j + 1) = Q_y \frac{x_2 - x_1}{\Delta t} W_y, \quad (3.13)$$

$$J_y(i, j) = Q \frac{y_2 - y_1}{\Delta t} (1 - W_x), \quad J_y(i + 1, j) = Q_x \frac{y_2 - y_1}{\Delta t} W_x, \quad (3.14)$$

where we define the parallel transport of the charge in 2d as <sup>7</sup>

$$Q_x \equiv U_x^\dagger(i, j) Q U_x(i, j), \quad Q_y \equiv U_y^\dagger(i, j) Q U_y(i, j). \quad (3.15)$$

One can easily check that this satisfies the lattice covariant continuity equation,

$$\dot{\rho}(i, j) = \sum_x U_x^\dagger(i - x) J_x(i - x) U_x(i - x) - J_x(i, j), \quad (3.16)$$

for sites  $(i, j), (i + 1, j), (i, j + 1)$ :

$$\dot{\rho}(i, j) = J_x(i, j) + J_y(i, j), \quad (3.17)$$

$$\dot{\rho}(i + 1, j) = U_x^\dagger(i, j) J_x(i, j) U_x(i, j) - J_y(i + 1, j), \quad (3.18)$$

$$\dot{\rho}(i, j + 1) = U_y^\dagger(i, j) J_y(i, j) U_y(i, j) - J_x(i, j + 1), \quad (3.19)$$

Eqs. (3.17), (3.18), (3.19) are consistent with the following definitions of the charge densities:

$$\rho(i, j) = Q(1 - x)(1 - y), \quad (3.20)$$

$$\rho(i, j + 1) = Q_y(1 - x)y, \quad (3.21)$$

$$\rho(i + 1, j) = Q_x x(1 - y). \quad (3.22)$$

However, since a particle's color charge depends on its path, so does  $\rho(i + 1, i + j)$  and we are not able to calculate it from the charge distribution itself. Rather, we directly employ covariant current conservation to determine the increment of charge at site  $(i + 1, j + 1)$  within the time-step. This way, we can satisfy Gauss's law in the non-Abelian case.

Finally, we have to check that  $\text{Tr}(Q^2)$  is conserved by this smearing method. This is true when the lattice spacing  $a$  is small, as the total charge of a particle is given by

$$Q_0 = Q(1 - x)(1 - y) + Q_x x(1 - y) + Q_y(1 - x)y + [a_p Q_{xy} + (1 - a_p) Q_{yx}] xy, \quad (3.23)$$

---

<sup>7</sup> We omit the term  $[A_z, J_z]$  here, because this term does not appear in 3d and because it does not matter for the present discussion.

where the  $a_p$  depend on the path of a particle and  $Q_{xy} = U_x^\dagger(i, j + 1)Q_y U_x(i, j + 1)$ ,  $Q_{yx} = U_y^\dagger(i + 1, j)Q_x U_y(i + 1, j)$ . If we require that  $\text{Tr}(Q_0^2)$  be constant, then the cross terms, for example  $\text{Tr}(QQ_x)$ , have to vanish. This is true when  $a$  is small, because  $\text{Tr}(Q[A, Q]) = 0$ :

$$\text{Tr}(QQ_x) = \text{Tr}(Q(Q + iga[A_x, Q] + \mathcal{O}(a^2))) = \text{Tr}(Q^2) + \mathcal{O}(a^2). \quad (3.24)$$

## IV. RESULTS

### A. Electrodynamics

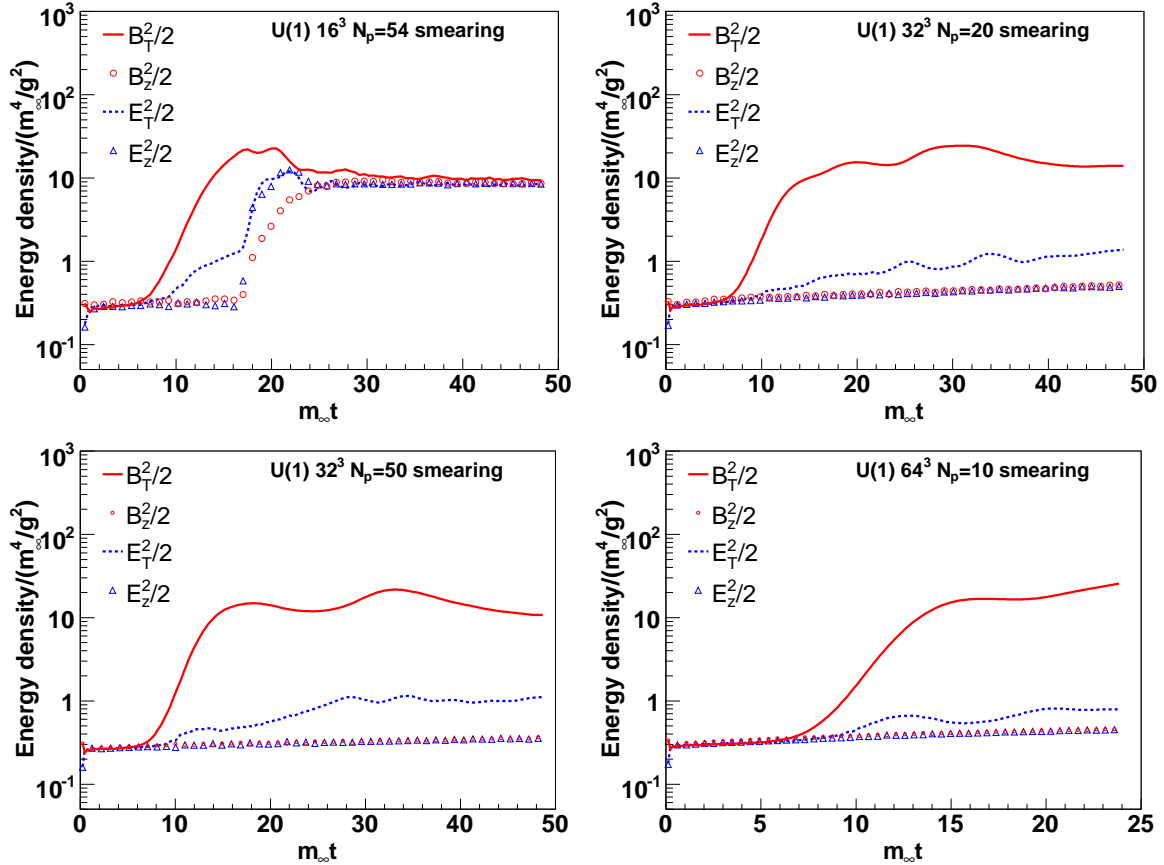


FIG. 3: Time evolution of the field energy densities for  $U(1)$  gauge group and anisotropic particle momentum distribution on various lattices. Simulation parameters in physical units are  $L = 5$  fm,  $p_h = 8$  GeV,  $g^2 n_g = 100$  fm $^{-3}$ ,  $m_\infty = 0.3$  GeV.

In Fig. 3 we show simulation results for “weak” fields with initial energy density on the order of  $0.1 m_\infty^4/g^2$ . For this case, we find that not only the transverse magnetic but also the transverse electric fields grow, albeit at a slower rate<sup>8</sup>. Note that here, and throughout the manuscript, squared transverse field components denote *averages* of squares of  $x$ - and  $y$ -components:  $B_T^2 = (B_x^2 + B_y^2)/2$ ,  $E_T^2 = (E_x^2 + E_y^2)/2$ . For the  $16^3$  lattice there is a very

<sup>8</sup> There is little difference to 1d-3v simulations, compare for example to Fig. 1 of ref. [37, 38, 39].

sudden growth of all field components at  $t \simeq 16 m_\infty^{-1}$  which we deem unphysical since we do not expect equi-partitioning of transverse and longitudinal fields; this is an example for the problems which arise in PIC simulations when the fields are very weak and the currents are not sufficiently stable. Indeed, this numerical instability disappears on larger lattices with more test-particles. The longitudinal field components are now essentially constant and only the transverse components grow. The time where the instability for the transverse magnetic fields sets in, as well as their growth rate and saturation point is quite similar for the  $32^3$  and  $64^3$  lattices.

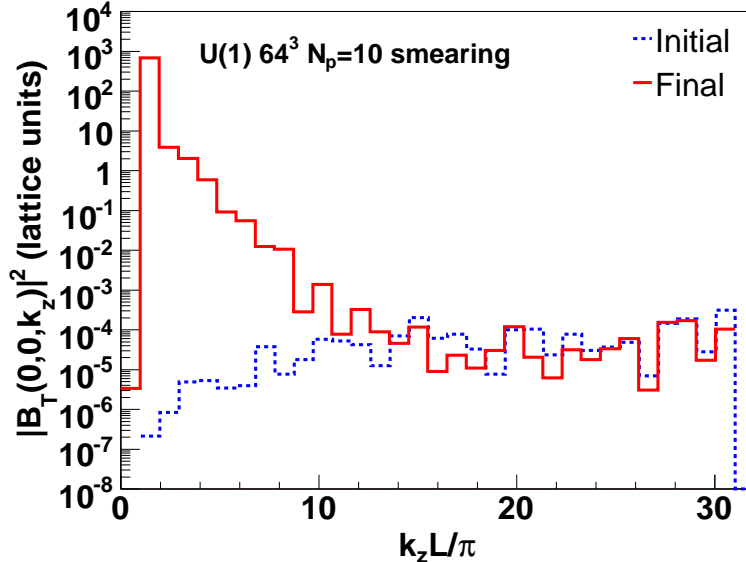


FIG. 4: Fourier transform of the transverse magnetic field from Fig. 3.

The slope of the exponential growth of  $B_T^2$  is about half that predicted by the hard-loop approximation ( $= \sqrt{2} m_\infty$  for the field energy density) which indicates that non-linear effects are not completely negligible. This is also apparent from the much slower growth of  $E_T$  as compared to  $B_T$  and in the Fourier transform of the transverse magnetic field shown in Fig. 4 which illustrates the spectrum of unstable modes. In the linear approximation, the spectrum of unstable modes for an extreme particle anisotropy as in eq. (2.10) extends to  $k = \infty$ . For the full non-linear solution, modes above  $k_z \simeq 12\pi/L$  are clearly stable.

## B. Chromodynamics

We now turn to simulations for the non-Abelian  $SU(2)$  gauge group. 3d-3v simulations within the hard-loop approximation show that the exponential growth of transverse magnetic and electric fields saturates at the scale  $m_\infty^2/g$  due to field self-interactions<sup>9</sup> [12, 13]. While we can not address such weak fields with PIC methods for  $SU(2)$ , we focus here on non-Abelian

<sup>9</sup> This, in fact, is true for moderate anisotropies where the typical longitudinal momentum is less than but comparable to the typical transverse momentum. For “extreme” anisotropies such as (2.10) the field strength is expected to grow larger, see discussion below.

plasma dynamics beyond the hard-loop approximation for initial field energy densities of  $\sim 10 m_\infty^4/g^2$  and above.

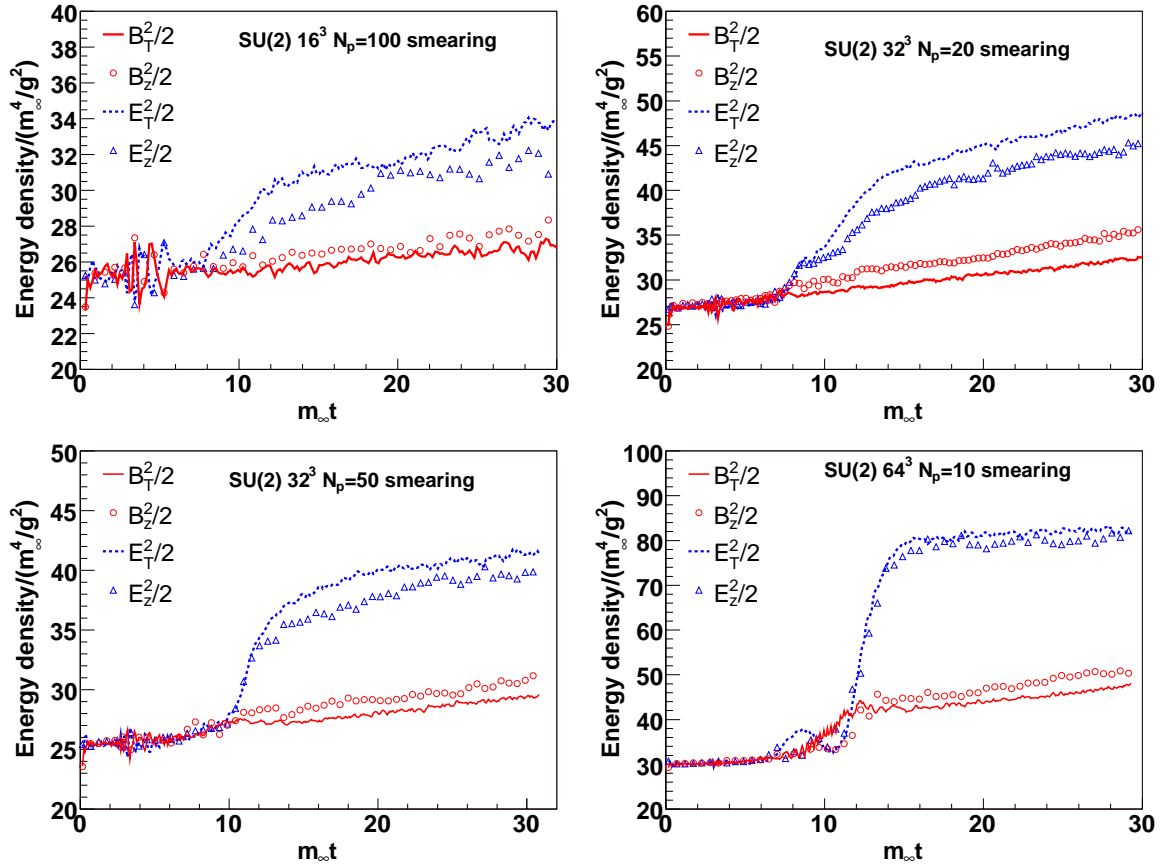


FIG. 5: Time evolution of the field energy densities for  $SU(2)$  gauge group and anisotropic initial particle momentum distributions. Simulation parameters are  $L = 5$  fm,  $p_{\text{hard}} = 16$  GeV,  $g^2 n_g = 10/\text{fm}^3$ ,  $m_\infty = 0.1$  GeV.

Fig. 5 shows results obtained on various lattices. We now do not find instabilities of transverse magnetic but of transverse and longitudinal *electric* fields, instead. However, the field growth shuts off much more rapidly than found above for weaker Abelian fields (note the *linear* scale in Fig. 5). A run with isotropic particle distribution, which we take as a test of the numerical accuracy, shows nearly constant fields over the time interval  $t \leq 30 m_\infty^{-1}$  as shown in Fig. 6. After the period of rapid growth of  $\mathbf{E}$ , both electric and magnetic fields settle to a slow linear growth with time, resembling somewhat the HL simulations shown in [12, 13]; however, the growth rate is comparable to that seen for isotropic distributions in Fig. 6 and so is within the numerical uncertainty.

Hence, we confirm that for 3d-3v simulations, even beyond the hard-loop approximation, the time evolution of non-Abelian fields stronger than  $\sim m_\infty^4/g^2$  differs from that in the (effectively Abelian) extreme weak-field limit. In particular, a sustained exponential growth is absent even during the stage where the backreaction on the particles is weak. It should be emphasized, in fact, that for very strong anisotropies a linear analysis predicts that the exponential field growth (in the weak-field situation) could perhaps continue until  $B^2 \sim m_\infty^4/g^2/\Delta\theta^2$ , with  $\Delta\theta^2 = p_z^2/p_T^2$  [23]. For our initial condition (2.10),  $\Delta\theta^2 = 0$  at  $t = 0$

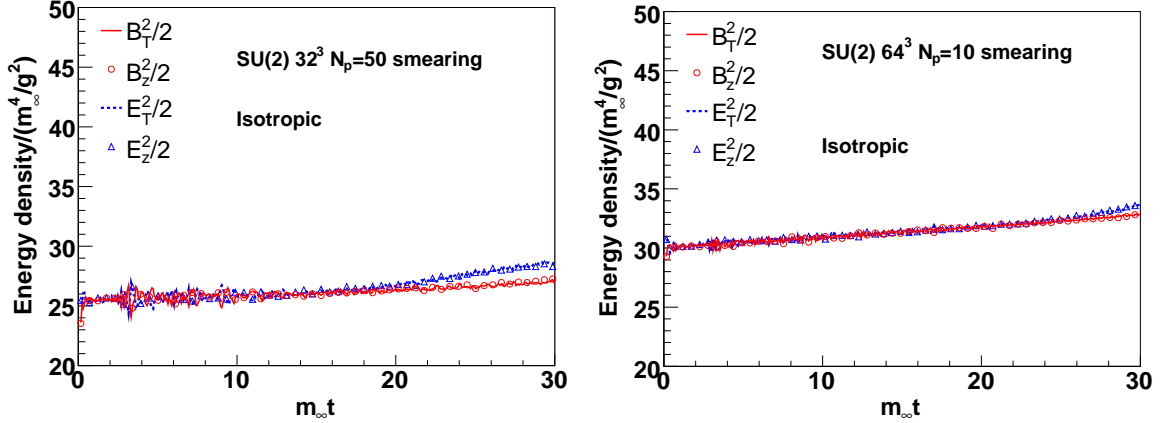


FIG. 6: Time evolution of the field energy densities for  $SU(2)$  gauge group and isotropic momentum distributions. Simulation parameters are the same as for Fig. 5.

but grows to  $\mathcal{O}(10^{-3})$  during the initial transient time with constant fields ( $t m_\infty \lesssim 10$  in Fig. 5) due to deflection of the particles. However, such strong fields are not seen in our PIC simulations.

The simulations of Fig. 5 indicate sensitivity to hard field modes at the ultra-violet end of the Brillouin zone,  $k = \mathcal{O}(a^{-1})$ , in contrast to the  $U(1)$  simulations shown above and to earlier 1d-3v  $SU(2)$  simulations [37, 38, 39]. The energy density of electric fields at late times doubles when going from a  $32^3$  to a  $64^3$  lattice with the same physical size  $L$ . Hence, the dynamics of  $SU(2)$  instabilities seen here is not dominated entirely by a band of unstable modes in the infrared but clearly involves a cascade of energy from those modes to a harder scale  $\Lambda$  [24]. However, the simulations shown in Fig. 5 indicate that  $\Lambda(t)$  grows to  $\mathcal{O}(a^{-1})$  during the period of rapid growth of  $\mathbf{E}$  or else the final field energy density should not depend on the lattice spacing.

In our PIC simulations the total energy of particles and fields is conserved, hence  $\Lambda(t)$  can not grow arbitrarily large if the energy density of the fields is UV sensitive. In three spatial dimensions, this is the case whenever the occupation number of hard field modes drops more slowly than  $\sim 1/k^4$ . The analysis of ref. [24], for example, suggests a  $\sim 1/k^2$  fall-off in the UV, which indeed corresponds to a quadratically divergent energy density as  $\Lambda \rightarrow \infty$ .

Although energy conservation will eventually stop the growth of the fields as the lattice spacing decreases further and further, it does not solve the following problem. When  $\Lambda(t) \sim 1/a$ , the hard field modes have reached the momentum scale of the particles,  $p_h = \mathcal{O}(a^{-1})$ , and so the clean separation of scales is lost, on which the approach (2.1,2.2) is based. In fact, since the occupation number (or phase space density) at that scale is of order 1 or less by construction<sup>10</sup>, it is inappropriate to describe modes at that scale as a classical field. Those perturbative modes should be converted dynamically into particles at a lower scale  $\Lambda_{f \rightarrow p} \ll 1/a$  so that the field energy density and the entire coupled field-particle evolution is independent of the artificial lattice spacing. We hope to be able to study this question in

<sup>10</sup> If not, the lattice was chosen too coarse to begin with, and the lattice evolution is far from the continuum limit.

the future.

Finally, we point out another interesting difference of the simulations from Fig. 5 to prior 1d-3v  $U(1)$  and  $SU(2)$  PIC simulations for weak fields [37, 38, 39] and to the present 3d-3v  $U(1)$  PIC simulations: the approximate isotropy of the gluon fields. For all but the present 3d-3v  $SU(2)$  PIC simulations transverse magnetic fields dominate, corresponding to an energy-momentum tensor of the form  $T_{\text{field}}^{00} \approx T_{\text{field}}^{zz}$  (and  $T_{\text{field}}^{xx} + T_{\text{field}}^{yy} \approx 0$ ). The results from Fig. 5, on the other hand, show that the energy transferred to “hard” field modes is distributed isotropically, regardless of the strong anisotropy of the particle momenta.

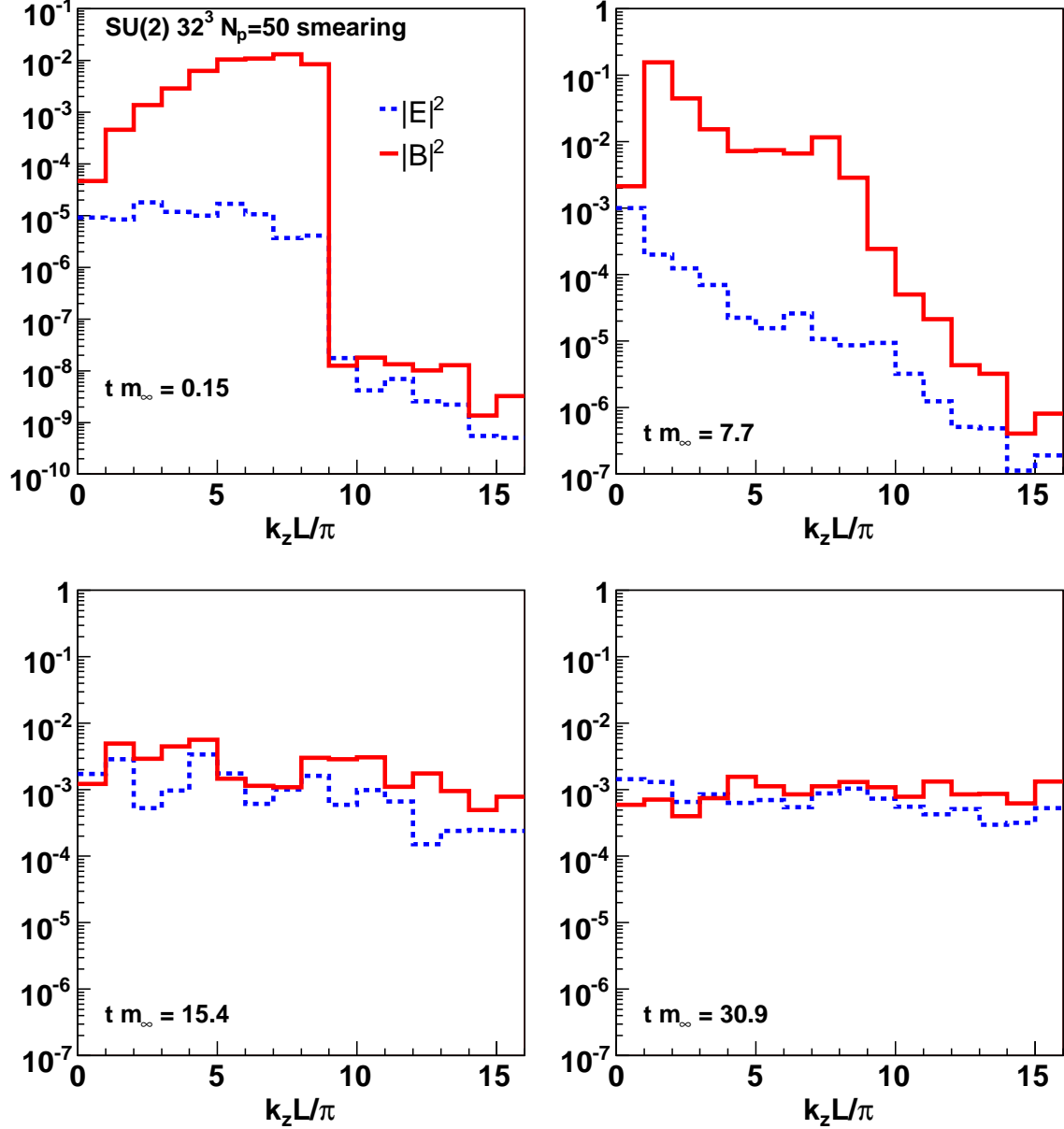


FIG. 7: Squares of the Fourier transformed (color-) electric and magnetic fields (in lattice units) at four different times. Simulation parameters are the same as for Fig. 5 but hard modes have been removed from the initial field configuration. Note that  $\pi/L \approx m_\infty$ .

One may wonder whether the sensitivity of the field evolution to the lattice spacing is indeed of dynamical origin, or whether it is in fact related to our initial field configurations. Since we pick the initial field amplitude randomly *at each site*, hard Fourier modes up to  $|k_i| = \pi/a$  do get populated (see also Fig. 4). We have therefore repeated the run on the  $32^3$  lattice with identical parameters except for removing the hard field modes from the initial field configuration<sup>11</sup>. We found that the subsequent field evolution was very similar to the one shown in Fig. 5 and so refrain from showing additional figures for the time evolution. Instead, in Fig. 7 we show  $\mathbf{E}^a(\mathbf{k}) \cdot \mathbf{E}^a(-\mathbf{k})$  and  $\mathbf{B}^a(\mathbf{k}) \cdot \mathbf{B}^a(-\mathbf{k})$  as functions of  $k_z$  at  $k_x = k_y = 0$ . Both are invariant only under global gauge rotations, while transformations which are not smooth over a spatial scale  $\sim L$  will redistribute power among modes. It may nevertheless illustrate how power is built up in the UV.

Before the onset of the rapid field growth seen in Fig. 5 (i.e.  $t m_\infty \lesssim 8$ ) we observe a relatively slow and gradual build-up of UV modes, in qualitative agreement with the discussion in ref. [24]. Also note the growth of the soft field modes with  $k_z \lesssim 5L/\pi$  at early times. This is the stage where the field evolution is independent of the lattice spacing. However, during the period of steep growth from Fig. 5 ( $10 \lesssim t m_\infty \lesssim 14$ ) the UV field modes build up very quickly and the distribution over  $k$  becomes flat. At present we do not have a detailed theoretical model for this nonlinear process which rapidly transfers power from the IR field modes to the scale  $k \sim 1/a \sim p_h$ . In the HL approximation, where  $\Lambda \ll p_h$  by assumption, it would take a parametrically very long time for the field modes to cascade energy all the way up to  $p_h$  since  $\Lambda(t) \sim m_\infty \sqrt{t m_\infty}$  [24].

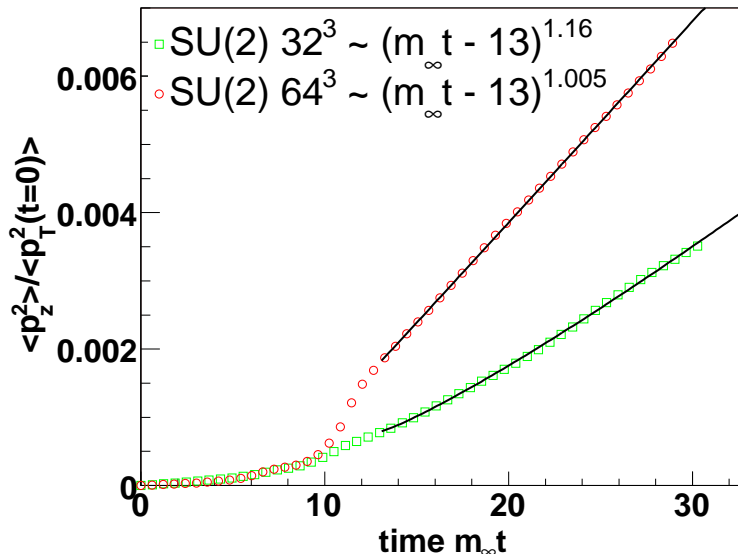


FIG. 8: Broadening of the longitudinal particle momentum distribution for the simulations from Fig. 5. The line represents the power-law fit from eq. (4.2).

Fig. 8 depicts the time evolution of the typical longitudinal particle momentum. The

<sup>11</sup> We have done this by Fourier transforming the initial  $\mathbf{A}$  fields, setting the occupation numbers of all modes above  $|k_{Li}| = \pi/2$  to zero, and finally transformed back to coordinate space. The original energy density was then restored by adjusting the field amplitude.

broadening of the longitudinal distribution during the initial transient  $t m_\infty \lesssim 10$  is *independent* of the lattice spacing. During the stage of steep field growth,  $p_z$  broadens more rapidly, especially for the finer  $64^3$  lattice. Since

$$\langle p_z^2 \rangle \sim t \frac{dN_{scatt}}{dt} q_z^2, \quad (4.1)$$

with  $q_z$  the typical momentum transfer in  $z$ -direction and  $dN_{scatt}/dt$  the collision rate of particles with the field modes, it follows that during this stage either the scattering rate and/or the typical momentum transfer increase. This observation (and the fact that the effect is much stronger for the  $64^3$  lattice) is consistent with the idea that during this stage the UV-cutoff  $\Lambda(t)$  for the classical field grows to  $\mathcal{O}(a^{-1})$ .

A power-law fit to the late-time evolution of  $\langle p_z^2 \rangle$  of the form

$$\frac{\langle p_z^2 \rangle}{\langle p_x^2 + p_y^2 \rangle} \propto t^\alpha, \quad (4.2)$$

yields  $\alpha \simeq 1$ , corresponding to a random walk of the particles in  $p_z$  with constant collision rate and average momentum transfer<sup>12</sup>. In an expanding metric, this should then lead to a  $\sim \tau^{-1/4}$  drop of the typical  $p_z$ , as argued by Bödeker [48] (see also section V in [23]). Hence, the anisotropy of the hard modes which develops in the early stage of a heavy-ion collision due to the rapid longitudinal expansion should be somewhat smaller than expected within the original “bottom-up” scenario [4], which predicted  $\sqrt{\langle p_z^2 \rangle} \sim \tau^{-1/3}$ .

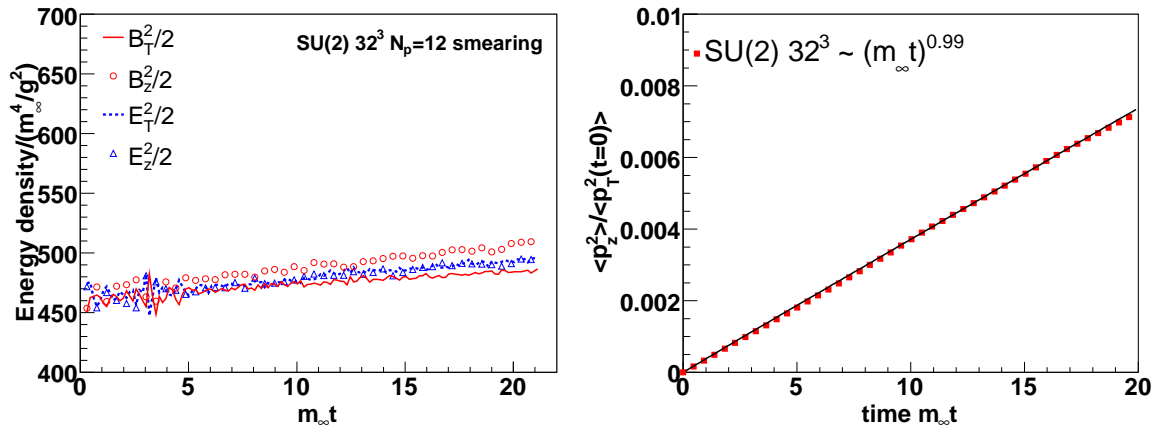


FIG. 9: Left: field evolution for stronger initial fields. Right: evolution of the average longitudinal particle momentum. The line represents the power-law fit from eq. (4.2). The remaining simulation parameters are  $p_h = 16$  GeV,  $g^2 n_g = 10/\text{fm}^3$ ,  $L = 5$  fm, as before.

For even stronger initial fields, we find that the growth rate of the electric fields and the dependence on the lattice spacing diminishes. Only a very mild linear growth remains over time spans which we can access in our simulations, see Fig. 9. A power-law fit of the form (4.2) again shows that the variance of the longitudinal momentum distribution

<sup>12</sup> Hence,  $\Lambda$  appears to be nearly constant in the late stages, which is natural if it has already grown to  $\mathcal{O}(a^{-1})$ .

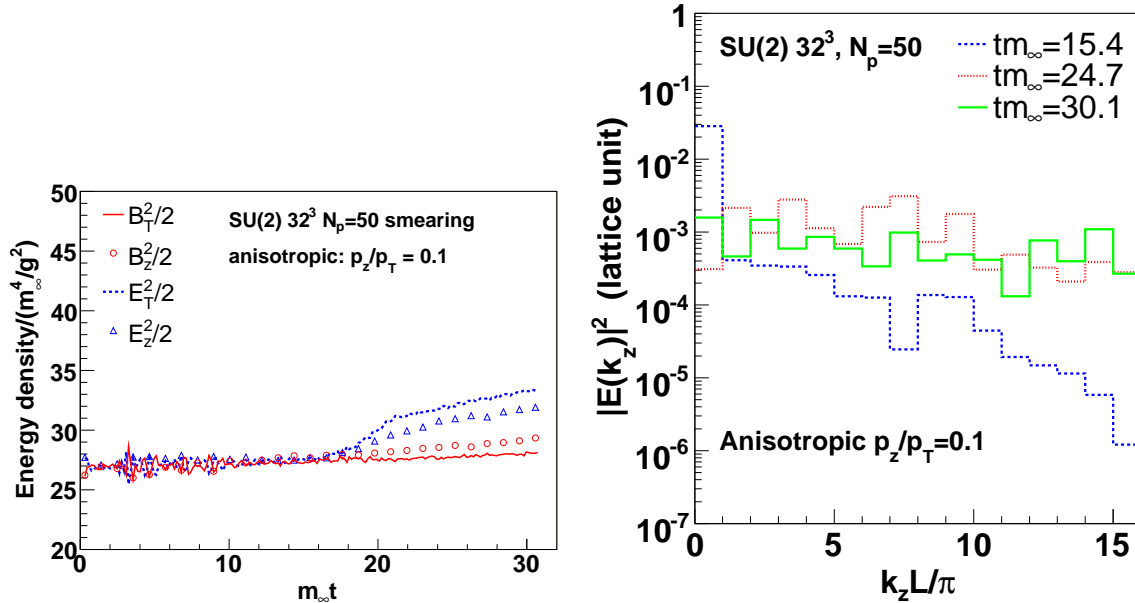


FIG. 10: Field evolution for moderate initial anisotropy,  $\sqrt{\langle p_z^2 \rangle / \langle p_T^2 \rangle} = 10\%$ . The remaining simulation parameters are the same as in Fig. 5. Left: field energy density as a function of time. Right: Fourier transformed color-electric fields (in lattice units) at three different times.

grows linearly in time, corresponding to a random walk of the particles in  $p_z$  with constant scattering rate (off the field modes) and typical momentum transfer.

We have also performed a simulation with a more moderate initial anisotropy of  $\sqrt{\langle p_z^2 \rangle / \langle p_T^2 \rangle} = 10\%$ , replacing the function  $\delta(p_z)$  in (2.10) by an exponential  $\sim \exp(-10 |p_z|/p_h)$ . The time evolution of the fields and of their Fourier transform is shown in Fig. 10. As expected, the onset of field growth is delayed, by roughly a factor of two, as compared to the simulation with extreme particle anisotropy. Also, the intermediate rapid growth of the electric fields is weakened since the rate of energy transfer from particles to fields is now lower. The late-stage field growth rate is comparable to that from Fig. 5. Nevertheless, even for this run with more moderate anisotropy, we observe that the nearly exponential suppression of hard field modes quickly turns into an approximately flat distribution at  $t m_\infty \approx 20$ , i.e. during the stage of rapid growth of the field energy density.

#### *Comparison with hard-loop results*

In Fig. 11 we present the dependence of the energy densities obtained by solving the soft-field equations of motion in the hard-loop approximation [13] for the case of  $\sqrt{\langle p_z^2 \rangle / \langle p_T^2 \rangle} \sim 0.1$ . For this simulation the initial condition has no fields, but instead has finite fluctuations of the auxiliary  $W$  fields which induce field fluctuations with typical initial energy density  $\mathcal{E} \sim 0.5 m_\infty^4/g^2$  at early times (for details of the initial condition and numerical algorithm used see Ref. [13]). Note that if one makes the same run with an isotropic hard particle distribution the fields remain isotropic and show no signs of growth.

As can be seen from Fig. 11 there is an initial period where no field growth occurs similar to the left graph in Fig. 10. At  $m_\infty t \sim 10$  all field components begin to grow isotropically

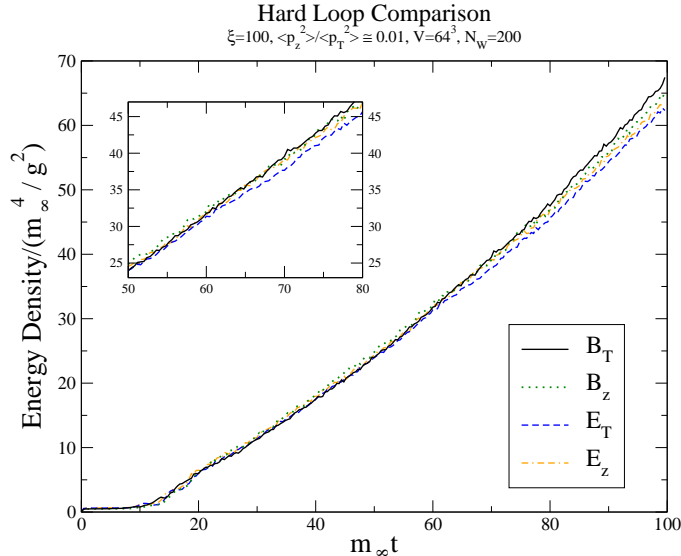


FIG. 11: Field evolution for moderate initial anisotropy as obtained from numerical solution of hard-loop effective theory [13].

in the hard-loop simulation. They then grow approximately linearly and isotropically for the duration of the run. At late times one can see a slight curvature upwards suggesting a faster than linear growth. This curvature is related to the finite discretizations used in both space-time and velocity space. Improving these discretizations or damping high angular momentum modes [12] extends the region in time over which the linear behavior is observed.

The inset of Fig. 11 shows the dependence of the field energy densities at late times when the magnitudes are comparable to those shown in Fig. 10. The rate of growth of the fields in the hard-loop simulations is approximately twice that of the WYM result if one compares the two at late times; however, given that the smeared-particle WYM results also show a slight linear growth in the isotropic case makes it hard to draw much from this observation. In addition, we see that for the most part the energy densities obtained in the hard-loop simulation are isotropic with only a slight preference for transverse magnetic fields at late times. In contrast, the WYM result shown in Fig. 10 shows a significant growth of electric fields. It is currently not understood in detail why the two simulations disagree on this basic point but, if true, points to large beyond hard-loop corrections to the field-particle dynamics of strongly anisotropic non-Abelian plasmas.

## V. DISCUSSION

We have presented numerical solutions of coupled particle-field dynamics in Abelian and non-Abelian gauge theories beyond the HL approximation. Such plasmas exhibit collective instabilities when the distribution of particles in momentum space is anisotropic (we restrict ourselves to an oblate distribution here). However, in the regime where field self-interactions can not be neglected, corresponding to field strengths of order  $\sim m_\infty^2/g$  and above, the evolution in chromodynamics is rather different from the one in Abelian plasmas. Most remarkably, for the initial conditions employed here we do not observe a period of sustained exponential growth of the soft fields. This is because the field modes can interact directly

and so the energy drained by the instability from the hard particles does not remain in unstable modes for a sufficiently long time.

The transition from exponential to linear growth at the scale  $m_\infty^2/g$  has been seen previously in 3d-3v simulations within the HL approximation [12, 13]. It appears that if the particles exhibit only weak anisotropy, that the HL approach could be continued (qualitatively) until the fields grow so large that they affect the particle motion significantly. Due to the small and constant energy transfer rate from particles to fields, this happens at very late times only.

However, for very anisotropic particle momentum distributions we find here that the evolution differs significantly from the HL simulations for field strengths of order  $m_\infty^2/g$  and above, even if overall the back-reaction on the hard particle modes is small. After some initial transient time, we observe a short period of rapid growth of (mainly electric) fields associated with an avalanche of energy into the UV. As long as the energy of the classical Yang-Mills fields is still much less than that of the particles, this avalanche proceeds to the smallest length scales, namely the lattice spacing  $a$  before reaching a steady-state distribution. Since  $1/a \sim p_h$ , this could perhaps be viewed as (partial) “classical decay” of the field into particles. The energy-momentum tensor of the fields is nearly isotropic at this stage, while Weibel instabilities seen in  $U(1)$  and 1d-3v  $SU(2)$  simulations lead to dominance of transverse magnetic fields.

When the very rapid UV avalanche has reached the end of the Brioullin zone of our lattice, the field growth rate drops again. From this point on, only a slow linear increase of the field energy density is seen, with similar growth rates for electric and magnetic fields. Also, if the initial field energy density is rather high, of order  $(10^2 - 10^3) m_\infty^4/g^2$ , then only this last stage of slow growth remains, where the mean-square width of the longitudinal particle distribution grows nearly linearly with time. This corresponds to a random walk with constant scattering rate (from the field fluctuations) and typical momentum transfer. The hard particle momentum distribution is still far from isotropic at this stage (unless the initial field energy density was comparable to that of the particles,  $\sim p_h n_g$ ).

Our simulations indicate that it could be important to implement a dynamical field to particle conversion at a scale  $\Lambda_{f \rightarrow p} < 1/a$ . It appears to us that this might lead to a continuous “cycle” of energy transfer from the anisotropic particles to soft field modes which then quickly re-emerges at the hard scale in isotropic form. The cycle should continue until all particle momenta are isotropic. Theoretically, it also remains to be understood why the energy avalanche from soft to hard field modes occurs so rapidly and whether this is related to chaoticity. In the future, we intend to perform more quantitative studies and verify the matching to the “bottom-up” solution for particle-field thermalization [49]. To do so, however, requires us to also allow for longitudinal expansion of the lattice and to include hard elastic scattering of particles.

**Acknowledgement:** M.S. thanks A. Rebhan and P. Romatschke for their collaboration. A.D. and Y.N. thank Larry McLerran for discussions and continuous encouragement to study non-perturbative particle-gauge field systems. Y.N. acknowledges support from GSI and DFG.

## APPENDIX A: MOMENTUM UPDATE

We consider the discretization of the equation

$$\frac{d\mathbf{p}}{dt} = gQ^a(\mathbf{E}^a + \mathbf{v} \times \mathbf{B}^a). \quad (\text{A1})$$

The difference form of the equation is

$$\frac{\mathbf{p}(t + \Delta t/2) - \mathbf{p}(t - \Delta t/2)}{\Delta t} = gQ^a \left( \mathbf{E}^a(t) + \frac{\mathbf{p}(t + \Delta t/2) + \mathbf{p}(t - \Delta t/2)}{2} \times \frac{\mathbf{B}^a(t)}{e(t)} \right) \quad (\text{A2})$$

Eq.(A2) can be solved by the Buneman-Boris method [40, 41] as follows:

$$\mathbf{p}(t) = \mathbf{p}(t - \Delta t/2) + \frac{\Delta t}{2} \mathbf{E}(t), \quad (\text{A3})$$

$$e(t) = |\mathbf{p}(t)|, \quad (\text{A4})$$

$$\mathbf{p}'(t) = \mathbf{p}(t) + \frac{\Delta t}{2} \mathbf{p}(t) \times \frac{\mathbf{B}(t)}{e(t)}, \quad (\text{A5})$$

$$\mathbf{p}_2(t) = \mathbf{p}(t) + \frac{2}{1 + (\mathbf{B}/e(t)\Delta t/2)^2} \frac{\Delta t}{2} \mathbf{p}'(t) \times \frac{\mathbf{B}(t)}{e(t)}, \quad (\text{A6})$$

$$\mathbf{p}(t + \Delta t/2) = \mathbf{p}_2(t) + \frac{\Delta t}{2} \mathbf{E}(t), \quad (\text{A7})$$

where  $\mathbf{E} \equiv gQ^a \mathbf{E}^a$  and  $\mathbf{B} \equiv gQ^a \mathbf{B}^a$ . This scheme is time reversible and the overall momentum integration is accurate to second-order in the time step.

- 
- [1] A. H. Mueller, Nucl. Phys. **A715**, 20 (2003), hep-ph/0208278.
  - [2] E. Iancu and R. Venugopalan (2003), hep-ph/0303204.
  - [3] L. McLerran, Nucl. Phys. **A752**, 355 (2005).
  - [4] R. Baier, A. H. Mueller, D. Schiff, and D. T. Son, Phys. Lett. **B502**, 51 (2001), hep-ph/0009237.
  - [5] S. Mrówczyński, Phys. Lett. **B314**, 118 (1993).
  - [6] S. Mrówczyński, Phys. Rev. **C49**, 2191 (1994).
  - [7] S. Mrówczyński, Phys. Lett. **B393**, 26 (1997), hep-ph/9606442.
  - [8] P. Romatschke and M. Strickland, Phys. Rev. **D68**, 036004 (2003), hep-ph/0304092.
  - [9] P. Arnold, J. Lenaghan, and G. D. Moore, JHEP **08**, 002 (2003), hep-ph/0307325.
  - [10] P. Romatschke and M. Strickland, Phys. Rev. **D70**, 116006 (2004), hep-ph/0406188.
  - [11] S. Mrówczyński, A. Rebhan, and M. Strickland, Phys. Rev. **D70**, 025004 (2004), hep-ph/0403256.
  - [12] P. Arnold, G. D. Moore, and L. G. Yaffe, Phys. Rev. **D72**, 054003 (2005), hep-ph/0505212.
  - [13] A. Rebhan, P. Romatschke, and M. Strickland, JHEP **09**, 041 (2005), hep-ph/0505261.
  - [14] A. Krasnitz and R. Venugopalan, Nucl. Phys. **B557**, 237 (1999), hep-ph/9809433.
  - [15] A. Krasnitz and R. Venugopalan, Phys. Rev. Lett. **84**, 4309 (2000), hep-ph/9909203.
  - [16] A. Krasnitz and R. Venugopalan, Phys. Rev. Lett. **86**, 1717 (2001), hep-ph/0007108.

- [17] A. Krasnitz, Y. Nara, and R. Venugopalan, Phys. Rev. Lett. **87**, 192302 (2001), hep-ph/0108092.
- [18] A. Krasnitz, Y. Nara, and R. Venugopalan, Nucl. Phys. **A717**, 268 (2003), hep-ph/0209269.
- [19] A. Krasnitz, Y. Nara, and R. Venugopalan, Nucl. Phys. **A727**, 427 (2003), hep-ph/0305112.
- [20] A. Krasnitz, Y. Nara, and R. Venugopalan, Phys. Lett. **B554**, 21 (2003), hep-ph/0204361.
- [21] T. Lappi, Phys. Rev. **C67**, 054903 (2003), hep-ph/0303076.
- [22] T. Lappi and L. McLerran (2006), hep-ph/0602189.
- [23] P. Arnold and G. D. Moore, Phys. Rev. **D73**, 025006 (2006), hep-ph/0509206.
- [24] P. Arnold and G. D. Moore, Phys. Rev. **D73**, 025013 (2006), hep-ph/0509226.
- [25] P. F. Kelly, Q. Liu, C. Lucchesi, and C. Manuel, Phys. Rev. Lett. **72**, 3461 (1994), hep-ph/9403403.
- [26] P. F. Kelly, Q. Liu, C. Lucchesi, and C. Manuel, Phys. Rev. **D50**, 4209 (1994), hep-ph/9406285.
- [27] J.-P. Blaizot and E. Iancu, Nucl. Phys. **B557**, 183 (1999), hep-ph/9903389.
- [28] S. G. Matinyan, E. B. Prokhorenko, and G. K. Savvidy, Nucl. Phys. **B298**, 414 (1988).
- [29] T. Kawabe and S. Ohta, Phys. Rev. **D41**, 1983 (1990).
- [30] T. S. Biro, C. Gong, B. Müller, and A. Trayanov, Int. J. Mod. Phys. **C5**, 113 (1994), nucl-th/9306002.
- [31] S. K. Wong, Nuovo Cim. **A65**, 689 (1970).
- [32] U. W. Heinz, Phys. Rev. Lett. **51**, 351 (1983).
- [33] M. Laine and C. Manuel, Phys. Rev. **D65**, 077902 (2002), hep-ph/0111113.
- [34] J. Ambjørn, T. Askgaard, H. Porter, and M. E. Shaposhnikov, Nucl. Phys. **B353**, 346 (1991).
- [35] C. R. Hu and B. Müller, Phys. Lett. **B409**, 377 (1997), hep-ph/9611292.
- [36] G. D. Moore, C.-r. Hu, and B. Müller, Phys. Rev. **D58**, 045001 (1998), hep-ph/9710436.
- [37] A. Dumitru and Y. Nara, Phys. Lett. **B621**, 89 (2005), hep-ph/0503121.
- [38] A. Dumitru and Y. Nara (2005), hep-ph/0511242.
- [39] Y. Nara (2005), nucl-th/0509052.
- [40] R. W. Hockney and J. W. Eastwood, *Computer Simulation Using Particles* (McGraw-Hill, New York, 1981).
- [41] C. K. Birdsall and A. Langdon, *Plasma Physics via Computer Simulation* (McGraw-Hill, New York, 1985).
- [42] J. W. Eastwood, Comput. Phys. Comm. **64**, 252 (1991).
- [43] J. W. Eastwood, W. Arter, N. J. Brealey, and R. Hockney, Comput. Phys. Comm. **87**, 155 (1995).
- [44] O. Buneman and J. Villasenor, Comput. Phys. Comm. **69**, 306 (1992).
- [45] T. Z. Esirkepov, Comput. Phys. Comm. **135**, 144 (2001).
- [46] T. Umeda, Y. Omura, T. Tominaga, and H. Matsumoto, Comput. Phys. Comm. **156**, 73 (2003).
- [47] O. Buneman, in *Computer Space Plasma Physics: Simulation Techniques and Software*, edited by H. Matsumoto and Y. Omura (Terra Scientific, Tokyo, 1993), pp. 67–84.
- [48] D. Bödeker, JHEP **10**, 092 (2005), hep-ph/0508223.
- [49] A. H. Mueller, A. I. Shoshi, and S. M. H. Wong (2005), hep-ph/0512045.